Additively Manufactured Foamed Polylactic Acid for Lightweight Structures

Abstract

Purpose- The study aims to make foamed Polylactic Acid (PLA) structures with different densities by varying deposition temperatures using the material extrusion (MEX) additive manufacturing process.

Design/methodology/approach- The extrusion multiplier (EM) was calibrated for each deposition temperature to control foaming expansion. Material density was determined using extruded cubes with the optimal EM value for each deposition temperature. The influence of deposition temperature on the tensile, compression, and flexure characteristics of the foamable filament was studied experimentally.

Finding- The foaming expansion ratio, the consistency of the raster width and the raster gap significantly affect the surface roughness of the printed samples. Regardless of the loading conditions, the maximum stiffness and yield strength were achieved at a deposition temperature of 200 °C when the PLA specimens had no foam. When the maximum foaming occurred (220 °C deposition temperature), the stiffness and yield strength of the PLA specimens were significantly reduced.

Practical implications- The obvious benefit of utilising foamed materials is that they are lighter and consume less material than bulky polymers. Injection or compression moulding is the most commonly employed method for creating foamed products. However, these technologies require tooling to fabricate complicated parts, which may be costly and time-consuming. Conversely, the MEX process can produce extremely complex parts with less tooling expense, reduction in energy use and optimised material consumption.

Original/Value – This study investigates the possibility of stiff, lightweight structures with low fractions of interconnected porosity using foamable filament.

Keywords: Additive manufacturing; Fused Deposition Modelling; Material Extrusion; Foamable Polylactic Acid Filament; Porous Structures; Lightweight Composite Beam

1. Introduction

There has been an increased interest in porous polymers in packaging, automotive, footwear and medical fields (Gama *et al.*, 2018). Porous polymers offer several benefits over bulkier polymer materials, including low density, thermal insulation, effective sound insulation, high specific strength, and corrosion resistance (Jin et al., 2019). The production of porous polymer is generally carried out using injection or compression moulding methods (Bharath Kumar *et al.*, 2016; Jayavardhan *et al.*, 2017). However, these methods necessitate tooling to create complex parts, which can be costly and time-consuming. There is a need for fabrication techniques that overcome the constraints of prior approaches, and additive manufacturing is considered a viable solution. The material extrusion (MEX) process is one of the most extensively utilised additive manufacturing techniques for producing prototypes and sophisticated functioning components with a great degree of design flexibility (Górski et al., 2015). The MEX technologies create the desired shape by staggering contoured layers on top of each other through an extrusion nozzle utilising a thermoplastic polymer such as Polylactic Acid (PLA), Acrylonitrile-Butadienestyrene (ABS), Polycarbonate, and Thermoplastic Urethane (TPU). This method offers several advantages, including low-cost equipment and raw material feedstock, simple post-processing and functionalisation using composites, and the flexibility to mix polymers (Das et al., 2017). In recent years, the interest in generating porous polymeric structures via MEX to produce low-density materials has grown significantly (Guddati *et al.*, 2019; Singh *et al.*, 2017; Yoo *et al.*, 2017).

Polymer foam is a porous polymer material containing many small voids/holes inside the polymer matrix. The basic method of making polymer foam generally starts with two materials: the blowing agent and the polymer itself (Kumar et al., 2016a). Blowing agents are classified as either physical or chemical based on the method of gas creation during the foaming process. Physical blowing agents (PBA) are liquids or gases that dissolve directly into the polymer matrix whereas chemical blowing agents (CBA) are often solids that dissolve or distribute before thermally decomposing to release gas (Coste *et al.*, 2020). Regardless of the foaming method, the following stages can be expected: firstly, the creation of the polymer/gas solution, followed by the nucleation of microcells, and secondly, cell growth and density reduction (Reglero-Ruiz et al., 2015). While a large range of CBAs are being sold commercially, many contain different ratios of the same base chemicals. The most common chemicals used to create these blowing agents are citric acid, sodium bicarbonate and azodicarbonamide (ADC) (David Eaves, 2004; Stehr, 2016). Choi *et al.*, (2020) used a mixture of CBA, a chain extender (CE) and PLA to create foamable filament for use in the MEX technology to manufacture scaffolds for medical applications. The optimal quantity of CE reaction was employed to improve the foam stability of PLA, rheological characteristics, mechanical properties, and molecular weight (here 1.5 wt %). CBA was used in the mixture to create a pore structure. Damanpack *et al.*, (2021) investigated the effect of the printing temperature and flow rate on the size of the bubbles and density of the *commercially*

available foamable filament. An analytical equation is presented to precisely replicate the experimental data on flow rate, density, and mechanical qualities in terms of printing temperature.

Syntactic foams are another category of porous polymeric structures which use hollow spheres in their matrix and have proven higher performance in MEX when compared to pure materials. Due to their specific properties, closed-cell foams are widely employed in underwater vehicles, aircraft parts and buoys (Kumar et al., 2016b). Customised characteristics can be achieved for many applications by varying the volume percentage of these hollow fillers in the matrix (Gupta and Ricci, 2006). H S et al., (2020) produced lightweight syntactic foam composites by mixing various content of micro glass balloons (GMBs) with high-density polyethylene (HDPE) using the MEX process and studied their rheological and mechanical properties. The results showed that the foam specimens produced have higher specific tensile and flexure modulus in comparison to pure HDPE. In addition, the loss modulus, storage modulus and complex viscosity increased by increasing GMB content.

Singh et al., (2018) showed that the tensile modulus of MEX-produced HDPE foams was higher than that of injection moulded specimens while density and fracture strain was lower. The printing resolution of the MEX machines is limited, and they would have difficulties producing micro-porosity smaller than 10 μm (Butscher et al., 2012). Another technique for making micro-porosity materials is to utilise a sacrificial template that may be dissolved or burnt off afterwards (Hammel *et al.*, 2014; Wu *et al.*, 2018). Song et al., (2018) fabricated hierarchical scaffolds with tailored macro/micro-porosity structures for bone tissue applications using a combination of the MEX process and gas foaming technology. In this procedure, a mixture of polyvinyl acetate (PVA) and PLA was utilised to form macropores, and subsequently, scaffolds were subjected to gas to create micropores. The results show that scaffolds with 100–800 μm macropores and 2-10 μm micropores could be accurately manufactured using the MEX technology. These new scaffolds have the potential to be utilised in bone tissue regeneration.

The work presented here aims to make foamed PLA structures with different densities by varying deposition temperatures using the MEX process. The extrusion multiplier (EM) was calibrated for each deposition temperature to control foaming expansion. The material density was calculated using MEX-fabricated cubes with optimum EM value for each deposition temperature. Experimental analyses were conducted to understand the effect of the deposition temperature on density, surface roughness, tensile, compression and flexural properties of the foamable filament. Moreover, the effect of infill percentage and EM on the non-foamed PLA and foamed PLA structures were assessed.

2.   Experimental Method

A commercial foam PLA (LW-PLA from Colorfabb) with a diameter of 1.75 mm was used. This filament contains an unknown quantity of the foaming ingredient, which is activated when the temperature exceeds a specified threshold. PLA specimens are produced using a Flashforge Finder MEX machine with a 0.4 mm nozzle. The geometry of the extruded samples is modelled using SolidWorks (V2021-22) software, and G-code for the MEX machine is generated using Simplify3D (V4.1.2) software.

In order to focus on the influence of the print temperature and foaming expansion, certain parameters such as layer height, extrusion speed, travel speed, top and bottom layers, perimeter shells, fill pattern and raster angle are kept constant. The EM and infill percentages were adjusted to regulate the quantity of material deposited. The infill percentage is a measure of the amount of material that fills the interior of the build, and the EM is a fractional scaling of the material flow rate through the nozzle. The fixed and variable parameters utilised in the studies are summarised in Table 1.

Table 1: Fixed and control factors for fabrication parameters

Fixed Factors		Control Factors	
Nozzle diameter (mm)	0.4	Temperature (℃)	200, 210, 220, 230 and 240
Extrusion speed (mm/s)	50		
Travel speed (mm/s)	80	Extrusion Multiplayer	From 0.9 to 0.4
Layer height (mm)	0.2		
Top and bottom solid layers	2	Infill Percentage (%)	100, 80, 50 and 20
Outline/perimeter shells	2		
Fill pattern	Rectilinear		
Raster angle	45/-45		

The hollow cubes with dimensions of $20 \times 20 \times 10$ mm with a wall thickness of 0.4 mm were fabricated to determine the best EM value at each printing temperature. The EM value was decreased from 1.0 in 0.05 increments until the thickness of the wall, measured with a digital micrometre (Mitutoyo, Japan), was within 0.05 mm of the 0.40 mm goal. In addition, solid cubes with the size of $10 \times 10 \times 10$ mm were fabricated to visually observe the quality and check the dimensional accuracy in comparison to the hollow cubes. The cubes with optimum EM values were used to calculate the density of the material for each temperature by measuring the dimensions and mass. For each temperature, three samples were tested, and average values were used.

Non-contact-based 3D Measuring Laser Microscope (Olympus OLS 5000), which has a display resolution of 0.5 nm, was used to capture microscopic photos. The OLS5000 microscope uses a 0.4 m diameter laser beam to scan the sample surface, allowing it to readily measure the surface roughness of samples. Arithmetic means deviation (Ra) and Arithmetical mean height (Sa) are the two most widely

Tensile, flexure and compressive PLA samples were manufactured according to ASTM D638-14, (2017), ASTM D790-10, (2016) and ASTM D695-15, (2016), respectively. Each sample set included three specimens for each category of process parameters. The orthogonal orientation notation specified in ASTM 52921 (ISO/ASTM52921-13, 2019) is used to specify sample orientations relative to the build plate. Tensile and flexure were fabricated in three directions YX (Flat), YZ (Side) and ZX (Vertical), as illustrated in Figure 1. For the compression test, samples were fabricated in YX and ZX directions. The dryer box (eSun, China) was used to reduce moisture absorption during the manufacturing process of the specimens.
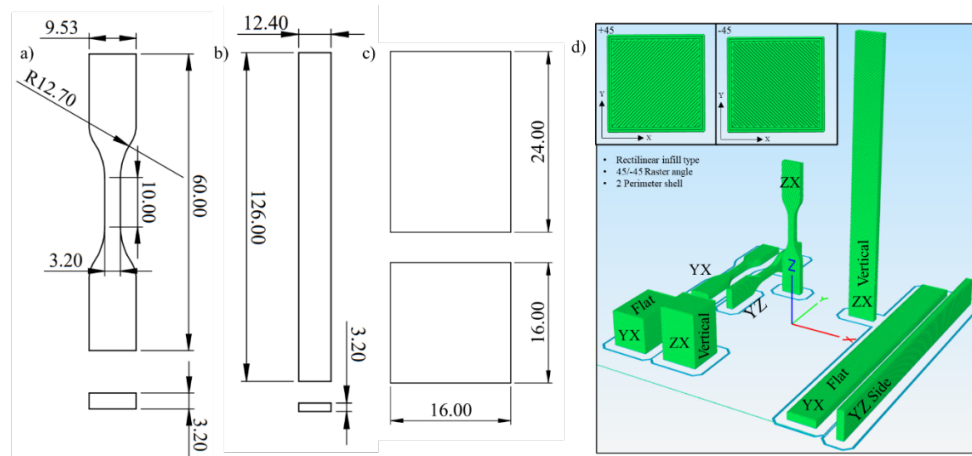

Figure 1: Standard samples for mechanical tests: (a) tensile, (b) flexure, (c) compressive. (d) 3D schematics showing orientations of printing line (The XYZ coordinate system gives the global orientation of the printing bed). All units are in mm.

The mechanical tests were performed using the universal electromechanical testing machine (Instron, USA) with 5 kN load cells for tensile and flexural tests and 100 kN for compression tests. Tensile and flexure specimens were tested at room temperature with a 2 mm/min fixed strain rate. Compression specimens were tested at room temperature with a 2.4 mm/min strain rate. The non-contact optical method (Imetrum system) was used to measure displacement and strain. All specimens were marked with white dots to be tracked by the camera, and the first pattern was used as the reference image, to which other images were compared (Figure 2). According to the ASTM standards referred to above, the experimental data were analysed to determine Young's Modulus, flexural modulus, tensile yield strength, compressive yield strength, and flexural yield strength. The linear portion of the stress-strain curve was used to determine Young's Modulus, and the slope was calculated using a linear fit. The flexural modulus of elasticity was calculated using the classical beam theory, with shear effects assumed to be minimal.
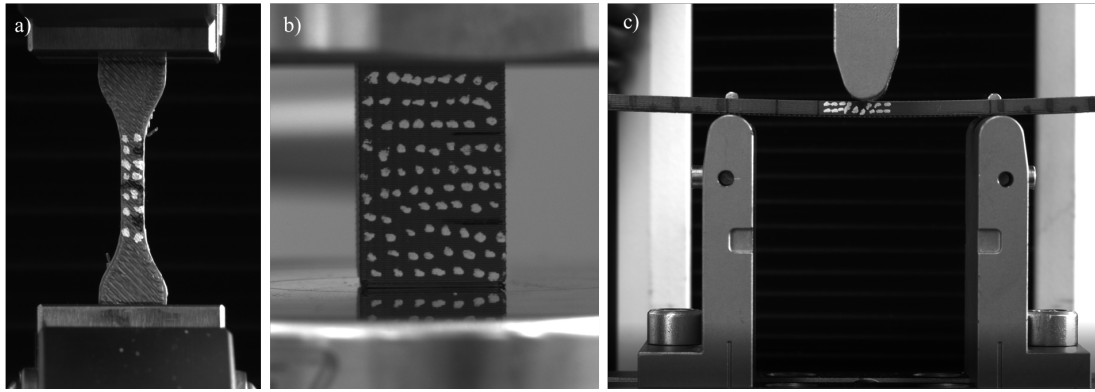
Figure 2: Mechanical testing of specimens (a) Tensile; (b) compression, and (c) flexural

3. Results and Discussion:

Figure 3 (a) depicts the effect of the EM on wall thickness. Extruding at 200°C, which is lower than the predicted temperature for foaming, and with an EM of 0.9 results in an accurate part. When the EM is reduced, the track width (wall thickness) is reduced below the fixed value of 0.4 mm. However, the EM must be reduced to accommodate substantial foam expansion while extruding at high temperatures.

The foam expansion depends on the temperature and flow rate, including nozzle size, layer height, and speed. In this study, the temperature is the only parameter that varies the amount of expansion as layer height, nozzle size, and speed is fixed, as shown in Table 1. There is an optimum processing temperature for achieving maximum expansion. The foam cannot be fully expanded if crystallisation occurs at the early stage of foaming before the dissolved blowing agent is entirely diffused out of the plastic matrix and into the nucleated cells. Conversely, when the temperature is too high, the solidification period is too prolonged, and the gas that has diffused from the plastic melt to the nucleated cells escapes from the foam (Naguib *et al.*, 2004).

As the filament melts at the hot end in the extruder head, foaming is to be expected at a higher temperature. Excess material will be expelled at the nozzle if the flow rate of filament to this cavity is too high to handle the foaming expansion. As a result, the actual track geometry will be enlarged for the desired track width, layer height, and head speed. The greater the foaming of the material, the lower the EM required to compensate for the higher volume expansion. The optimal EM for the foamable filament was defined when dimensional accuracy was less than ±0.05 mm in the hollow cubes and ± 0.5 mm for the solid cube from the target, as shown in Figure 3 (a) and (b), respectively, as good as could be achieved using the available MEX machine. The ideal EM and density at each temperature are shown in Figure 4 (a), with the lowest density, or maximum expansion, occurring at 220 °C. Foam expansion at a density of 0.59 g/cc results in a maximum volume increase of 110%, which is lower than the 150% reported by Hermann, (2020).

Figure 5 shows microscopic pictures of extruded foamable filament at different temperatures. Despite the fact that there is evidence of a small degree of foaming as blister-type structures observed on the

filament extruded at 200°C, the samples at this temperature are considered to be non-foamed as there are insufficient air bubbles to provide foamed characteristics. When extruding at a higher temperature, the blisters become more widespread and appear as near-spherical bubbles resulting in a significantly roughened surface.

There is a distinct raster gap in the necking area in extruded samples at 200 °C, and the measured raster width is considerably close to the set value (0.4 mm) in the slicer software. Conversely, it becomes significantly more difficult to differentiate between raster lines in the printed samples at higher temperatures due to foaming expansion which fills the raster gap (necking area) between two raster lines. Moreover, the width of the raster lines is slightly higher than the set value and changes based on the extrusion temperature as the amount of foaming expansion changes. It is noteworthy to mention that the samples extruded at 240 °C provided the most inconsistent raster width, which resulted in the bigger raster gap in some sections. This can be justified as the gas that has diffused from the plastic melt to the nucleated cells escapes from the foam when the temperature is too high and the solidification period is too lengthy (Naguib *et al.*, 2004). As a result, the foam will shrink, lowering the volume expansion ratio.

The mean of the average height difference for the average plane (S_a) and the average surface (R_a) ensure stable results since the parameter is unaffected by scratches, contamination, or measurement noise. As is clear from Figure 4 (b), the profile (both in X and Y directions) and areal roughness are doubled when the foaming occurs at temperatures above 200 °C. The surface roughness of extruded samples at 210 °C and 230 °C is slightly lower than that at 220 °C. This can be justified by the smaller foaming expansion at these temperatures. Even though samples at 240 °C have smaller foaming expansion in comparison to those at other extrusion temperatures, the inconsistent raster line width and bigger raster gaps increase the surface roughness at this temperature.

Figure 3: Hollow and solid cubes; (a) Measuring wall thickness of the hollow cube; (b) Solid cubes printed with different EM values for four different deposition temperatures
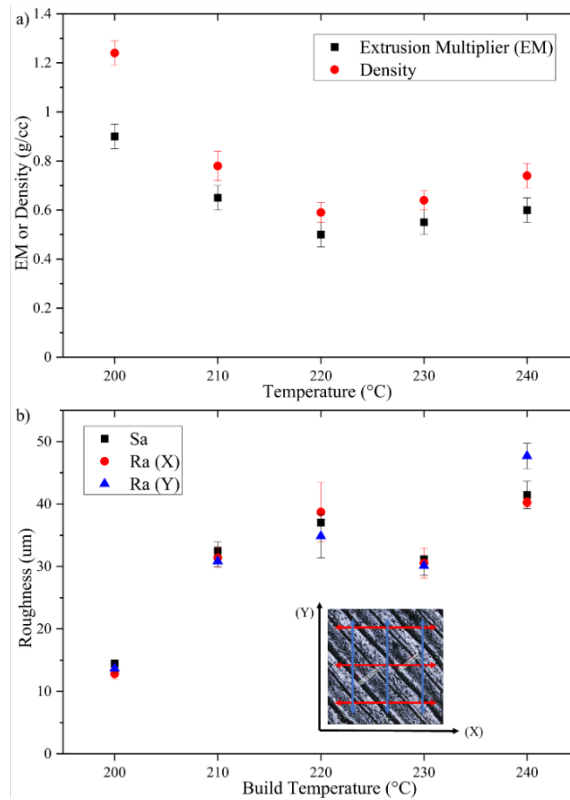

Figure 4: (a) Ideal EM and density for five different temperatures; (b) The profile and areal roughness of the extruded parts at the different deposition temperature
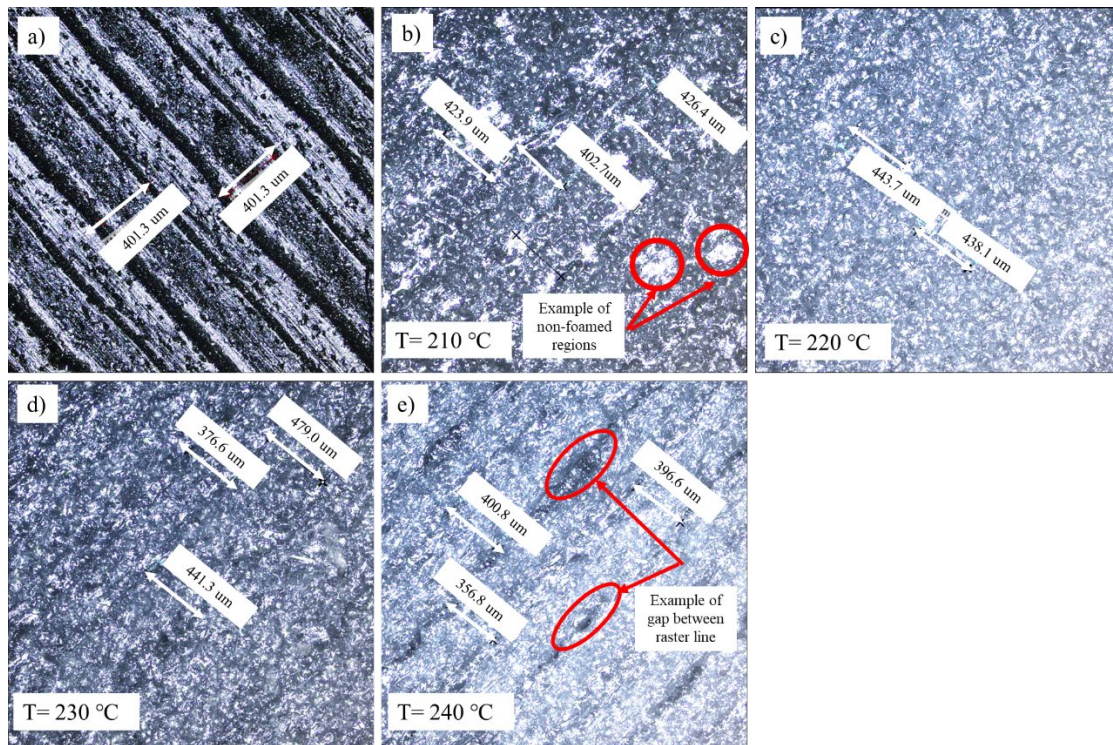
The maximum stiffness and yield strength, as presented in Figure 6 (a) and Figure 6 (b), respectively, were achieved at 200 °C extrusion temperature when there was no foam in the specimens. Conversely, Young's modulus was reduced significantly when the maximum foaming occurred in the specimens at 220 °C extrusion temperature. The Young modulus's and tensile yield strength followed the same trend concerning the extrusion temperature regardless of the build orientation. The YX (Flat) and YZ (side) test results were similar and within engineering scatter at the deposition temperatures above 200 °C. However, the specimens in the ZX direction had significantly lower stiffness and yield strength than those in the YX and YZ directions (a similar phenomenon is observed by Chacón et al. (Chacón *et al.*, 2017)), regardless of the deposition temperature. In ZX specimens, the cross-sectional layers were stacked up perpendicular to the applied force, and separation happened at the interface between two stacked layers, which resulted in lower strength and stiffness. A slightly higher deviation of yield strength for the ZX samples was due to difficulty controlling foaming expansion for the tensile samples' small cross-sectional area, which resulted in dimensional measurement inaccuracy.
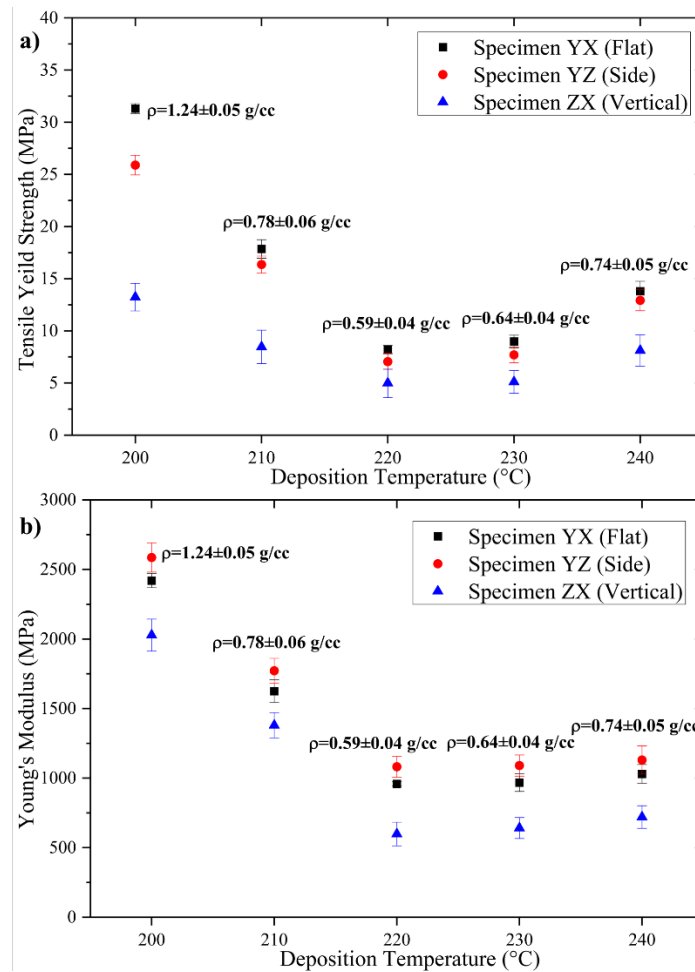
Figure 6: Tensile (a) Yield strength and (b) stiffness of tensile specimens for different temperatures and build orientations

The maximum compressive yield strength was achieved with non-foamed PLA at 200 °C in both directions (flat and vertical), as shown in Figure 7, similar to the tensile results presented in Figure 6 (b). Conversely, the minimum compressive yield strength and stiffness were obtained for foamed PLA at 220 °C in the YX direction and 230 °C in the ZX direction. The yield strength almost remained constant at higher temperatures after maximum foaming expansion (220 °C), while stiffness slightly improved. This is in contrast with tensile yield results where the strength of PLA increased at a higher temperature when the density increased or, in other words, the amount of foaming expansion decreased. Changing print direction from YX to ZX did not significantly affect the compressive yield strength at 200 °C. However, the compression yield strength was reduced by 25%, 40%, 58.7% and 33.9% at 210 °C, 220°C, 230 °C and 240 °C, respectively. The foam samples are more sensitive to the direction of material deposition because of the irregular surface of the tracks. As a result, their performance is determined by the orientation of the raster lines (width or height) in proportion to the applied force, as well as the quality of the bonding region between the raster lines (Abbott *et al.*, 2018).

There is a bigger gap between stiffness values obtained from compression and tension in non-foamed PLA in comparison to the foamed PLA. The stiffness value obtained from the compression test in YX and ZX directions is 2966 ± 300 MPa and 2960 ± 250 MPa at 200 °C, respectively, which is greater by

18.4% and 31.8% compared to the stiffness obtained from tensile specimens. The poor performance of the tensile specimens in the ZX direction can be justified by the nature of the extruded parts, which are layer-by-layer based. In the ZX direction, these layers are perpendicular to the tensile force and can be easily pulled apart from each other due to the weak interface bond between layers, whilst under compression loading, these layers crush or compress on each other. Conversely, a better agreement is achieved between tensile and compression stiffness for foamed PLA. For instance, at the maximum foaming expansion (220 °C), the stiffness value obtained from the compression test is 1028 ± 22.7 MPa in the YX direction and 581 ± 19.5 MPa in the ZX direction, which only varies by 6.8% and 2.92%, respectively, compared to the stiffness obtained from tensile specimens.
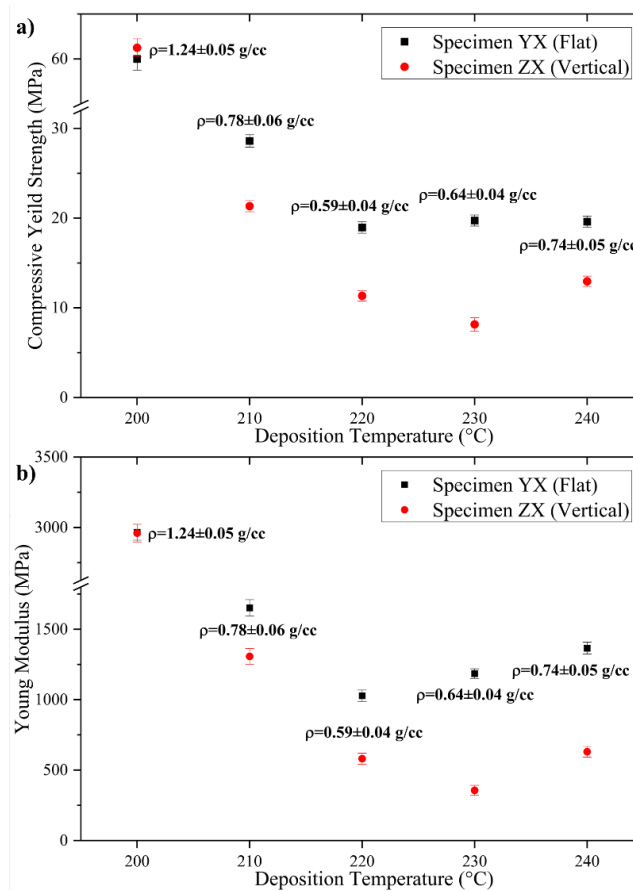

Figure 7: Compressive (a) yield strength and (b) stiffness for different temperatures and build orientations

Figure 8 shows three flexural test data on the PLA filament for five different deposition temperatures in three different build directions. The deflection at which maximum load occurs was calculated at 6 mm based on ASTM D790 (D790-10, 2016). The foam PLA samples were flexible enough not to break, while normal PLA experienced some cracks, but the outer shell held together. A first glance at the flexural modulus and flexural strength results show a similar trend to tensile results with maximum and minimum stiffness/strength at 200 °C and 220 °C, respectively. Although extruded samples in the YX direction (on the largest side of the samples) resulted in the highest tensile and compressive yield strength, the highest flexural modulus and flexural strength were achieved in the YZ direction (on the

long thin side of the samples). This can be justified as perimeters, and the weak interface between layers is positioned parallel to the tensile and compressive forces at the top and bottom of the specimens, which cannot be easily pulled away from each other. On the other hand, Similar to the compressive and tensile test, samples in the ZX direction provided the lowest flexural modulus and strength. This is due to the fact that the layers are orientated perpendicular to the flexural forces, where tensile and compressive forces can pull or compress the weak interface between layers.

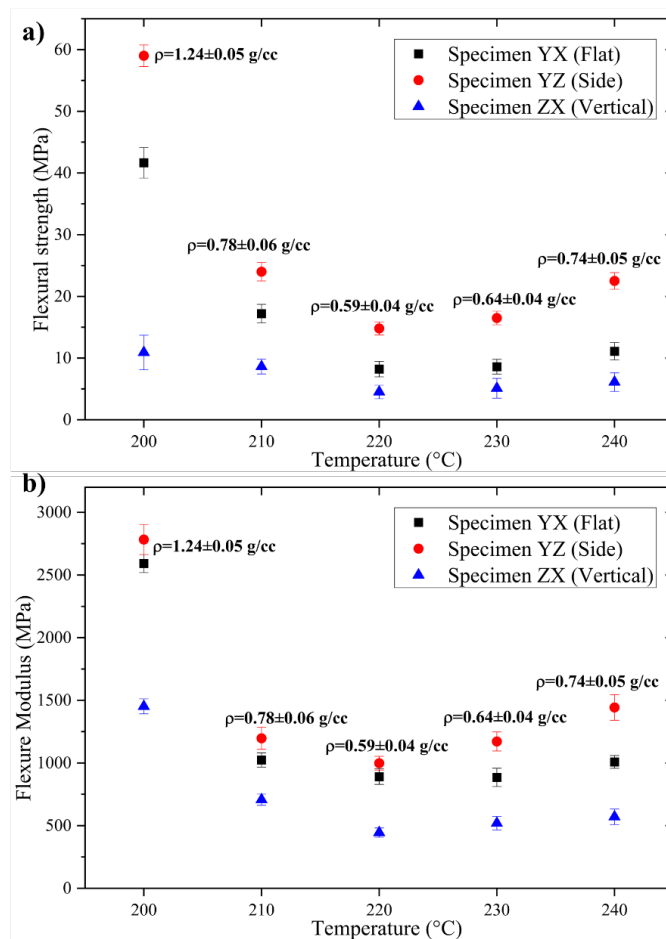The summary of the experimental results for tensile, compression and flexure tests can be found in Table 2.

Figure 8: (a) flexural strength and (b) flexure modules for different temperatures and build orientations

12

Temp (°C)	Print Direction	Tensile		Compression		Flexural	
		E (MPa)	σ_y (MPa)	E (MPa)	σ_y (MPa)	E (MPa)	σ_y (MPa)
200	YX	2420 ± 51	31.31± 0.47	2966±56.5	60.0±1.25	2591 ± 72	41.6± 2.5
	YZ	2586±105	25.89±0.95	--	--	2783±120	59±1.7
	ZX	2028±115	13.23±1.32	2960±62.5	61.3±0.91	1452±60	10.9±2.8
210	YX	1625±81	17.2±1.5	1651±58.5	28.6±0.68	1024±56	17.2±1.5
	ZX	1771±89	16.35±0.82	--	--	1197±88	24±1.5
	YZ	1380±91	8.46±1.6	1307±56.5	21.3±0.62	707±45	8.62±1.2
220	YX	958 ± 15.89	8.20 ± 0.29	1028±22.7	19.0±0.65	878 ± 14	8.13 ± 0.3
	ZX	1081±76	7.05±0.8	--	--	998±54	14.8±1.0
	YZ	598±85	4.99±1.4	581±19.5	11.5±0.28	444±37	4.5±1.1
230	YX	967±63	8.6±1.2	1185±34.4	19.7±0.61	885±73	8.6±1.2
	ZX	1090±76	7.7±0.77	--	--	1171.5±76	16.5±1.1
	YZ	641±75	5.11±1.1	324±16.0	8.2±0.17	519±54	5.1±1.6
240	YX	103±66	11.1±1.4	1366±41.5	19.6±0.61	1008±51	11.1±1.4
	ZX	1130±101	12.9±1	--	--	1443±101.7	22.5±1.3
	YZ	720±81	8.12±1.5	630±18.0	13.0±0.38	570±62	6.1±1.5

The effect of four different infill percentages (20%, 50%, 80% and 100%) were investigated on foamed, and non-foamed PLA printed samples. Two deposition temperatures that provided no foaming (200 °C) and maximum foaming (220 °C) were chosen to fabricate tensile, compression and flexural samples in the YX direction. All the samples were fabricated using the process parameters presented in Table 1.

Figure 9 shows the linear relationship between infill percentage and density of the foamed and non-foamed structures with two different deposition temperatures. It is clear that regardless of the infill percentage, the density of the non-foamed PLA is almost double that of foamed PLA. Another noteworthy observation was that the density of the foamed PLA at 80% infill almost equals the density of non-foamed PLA at 20% infill (0.5 g/cc vs 0.49 g/cc, respectively).
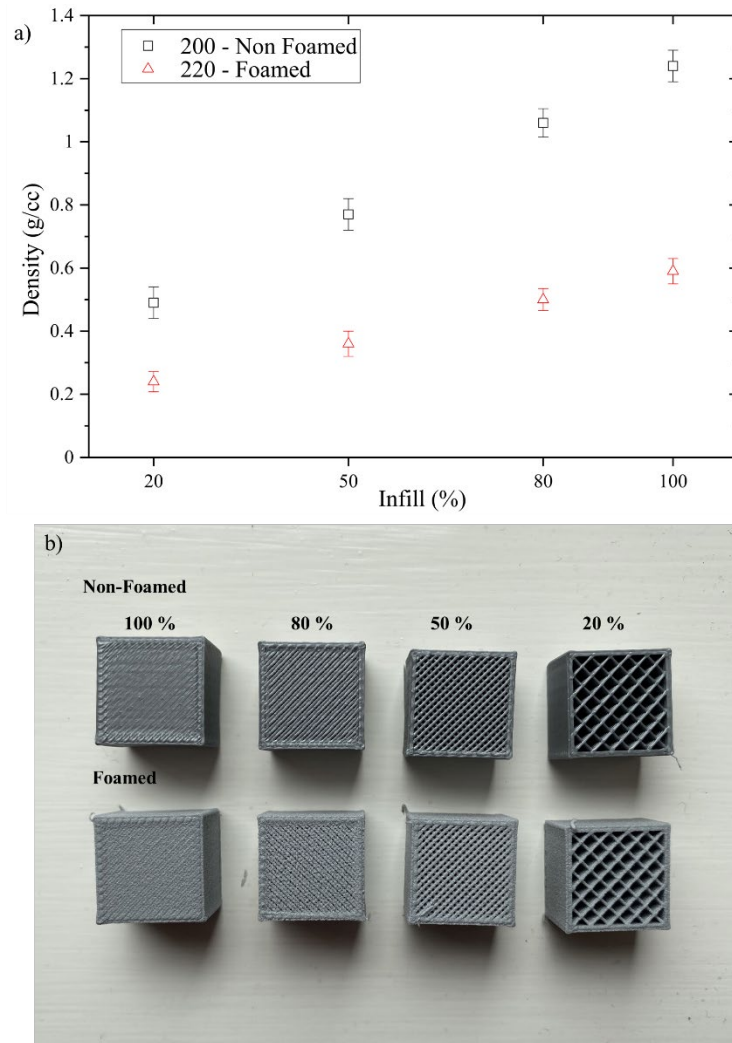
Figure 9: (a) The effect of the infill percentage on the density of the foamed and non-foamed PLA (b) the representative cubes with different infill and EM values

Figure 10 shows the effect of the infill percentage on the tensile, compressive and flexural yield strength of non-foamed and foamed PLA. As expected, the solid samples had the maximum mechanical strength, while low infill structures (20% filling content) had the least, regardless of the PLA types (foamed or non-foamed). This can be explained as the higher infill percentage increased the density of the connections and provided smaller porosity in the structure. In addition, the general trend showed that the tensile and compressive yield strength of non-foamed and foamed PLA were close to each other at lower infill percentages, whereas the difference was increased significantly at 100% infill. This happens as the amount of strength obtained by increasing the infill proportion does not grow linearly.

In non-foamed PLA samples, the compression yield strength was reduced by almost twice as much as the tensile yield strength when the infill percentage was reduced from 100% to 80% in the extruded samples. This can be attributed to the inner walls of the low infill structure failing due to localised buckling as they were not aligned with respect to the compressive load.

In the foamed PLA samples, the yield strengths were reduced by approximately 18% for tensile and flexural samples and 27% for compression samples when the infill percentage was reduced from 100% to 80%. However, when the infill percentage was reduced from 80% to 50%, the compressive yield strength was reduced by 64%, which is significantly higher than the 30% reduction in tensile yield strength.

As indicated, the density of the non-foamed PLA cube with 20% infill was close to the density of the foamed PLA cube with 80% infill. However, the strength of these two print specifications showed no similarity. The average tensile yield strength of the foamed PLA specimens with 80% infill was lower by 57% in comparison to the non-foamed PLA specimens with 20% infill (6.67 and 15.5 MPa, respectively). Conversely, the average compressive yield strength was higher by 38% in foamed PLA specimens with 80% infill compared to the non-foamed PLA specimens with 20% infill (13.78 and 8.5 MPa, respectively). This can be associated with foaming expansion (gas bubbles) that create empty spaces (voids) inside raster lines. These voids negatively affected tensile samples as the crack tends to initiate at the weak areas under tensile load. In contrast, these voids locally absorb mechanical energy in compression specimens and prevent local buckling in the inner walls under compressive load.

The average flexural yield strength was lower by 52% in the foamed PLA specimens with 80% infill than the non-foamed PLA specimens with 20% infill (6.7 and 14 MPa, respectively). The presence of the voids caused a stress concentration, weakening the beam at the outermost surface where the tension is at the maximum point resulting in lower flexural strength of the foamed PLA.
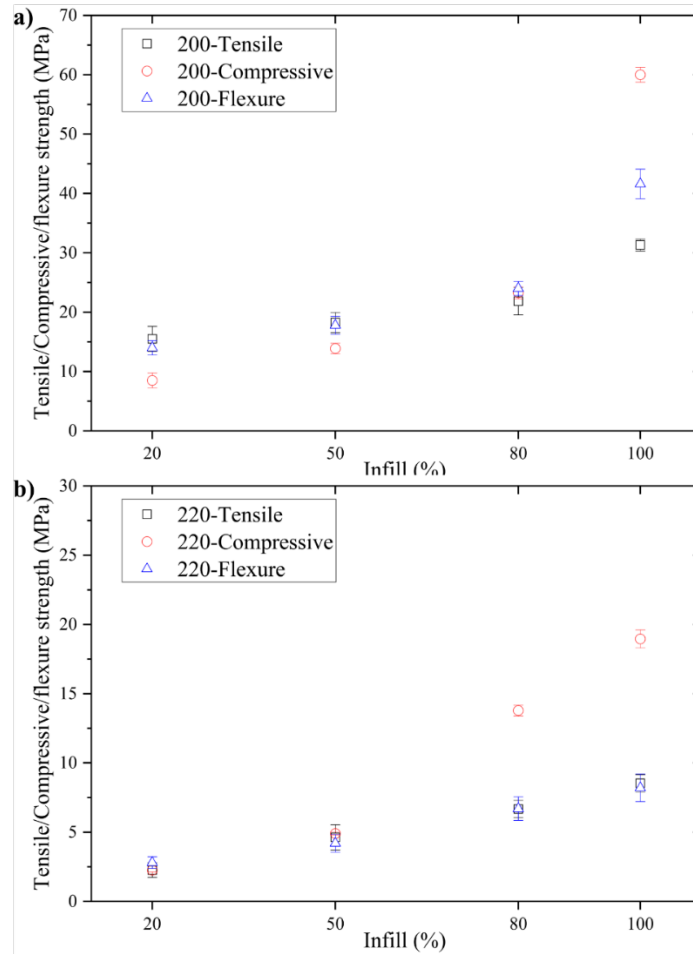
Figure 10: The effect of infill percentage on the strength of (a) non-foamed and (b) foamed PLA

In non-foamed PLA, when the infill percentage was reduced from 100% to 80%, the stiffness was reduced by 3.3% and 24% for tensile and compression samples, respectively, as illustrated in Figure 11 (a). A greater stiffness reduction was observed for both tensile and compressive specimens (26% and 49%, respectively) when the infill percentage was reduced from 80% to 50%. This can be justified as the lower infill densities can result in more voids and porosity inside the structure resulting in lower stiffness. Other factors such as the quality of bonding between raster lines and the amount of material used in the structure play significant roles in the stiffness value. Despite the fact that the tensile samples' stiffness experienced a small reduction (6.7%) when the infill percentage was reduced from 50% to 20%, the stiffness in the compression specimens was reduced significantly by 37.8%.

In foamed PLA specimens, the compression and tensile stiffness were significantly close to each other for 100% and 80% infill. However, further reducing the infill percentage from 80% to 50% reduced stiffness in compression specimens more than tensile specimens (49% vs 11% respectively). The same trend was followed when the infill percentage was reduced from 50% to 20% but with a considerably higher reduction of stiffness in tensile and compression specimens (30% vs 43%, respectively).

The comparison of average stiffness for the non-foamed samples with 20% infill and foamed samples with 80% infill showed a similar trend to Figure 10. The stiffness for tensile and flexural of non-foamed samples with 20% infill is higher by 45% and 20% compared to the foamed samples with 80% infill. On the other hand, foamed specimens with 80% infill had 9% higher compression stiffness than non-foamed specimens with 20% infill.
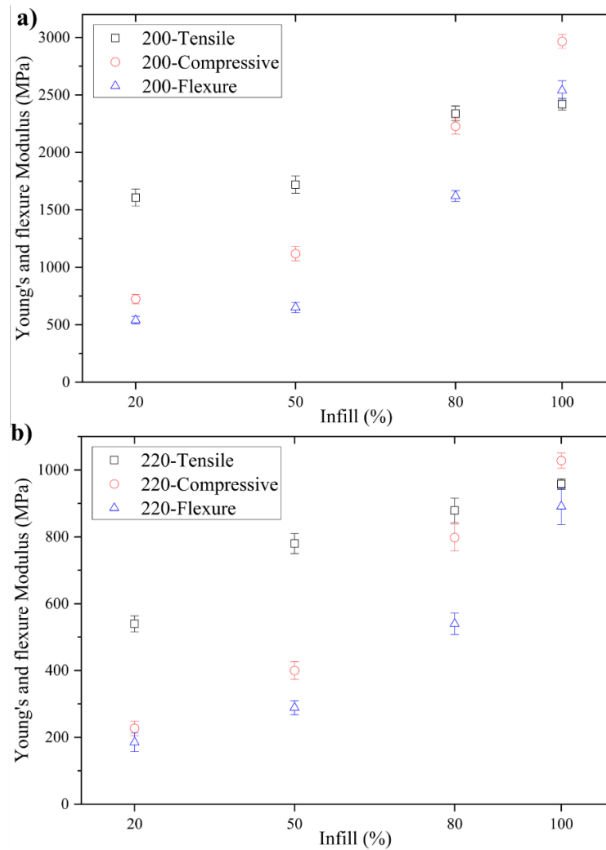

Figure 11: The effect of infill percentage on the stiffness of (a) non-foamed and (b) foamed PLA

Table 3 summarises the material properties for tensile, compression and flexure tests for different infill percentages at the no-foaming (200 ℃) and maximum foaming (220 ℃) nozzle temperatures.

Table 3: The summary of the experimental results for different infill percentage

Infill %	Temp (℃)	Tensile		Compression		Flexural	
		E (MPa)	σ_y (MPa)	E (MPa)	σ_y (MPa)	E (MPa)	σ_y (MPa)
100	200	2420 ± 51	31.31± 0.47	2966±57	60.0±1.25	2591 ± 72	41.6± 2.5
	220	958 ± 15.9	8.20 ± 0.29	1028±23	19.0±0.65	878 ± 14	8.13 ± 0.3
80	200	2338±64	21.84±2.3	2227±67	23.27±1	1620±47	24±1.2
	220	879 ± 37	6.67±0.62	798±40	13.78±0.39	540±32	6.7±0.85
50	200	1720±75	18.24±2.3	1119±62	13.88±0.89	650±45	17.8±1.5
	220	780 ± 30	4.62±0.92	400±27	4.9±0.1	288.6±21	4.2±0.64
20	200	1607±62	15.5±2.1	724±41	8.5±1.25	540±32	14±1.2
	220	540±24	2.26±0.52	227±22	2.25±0.1	185.2±28	2.8±0.42

The foam material must be extruded in solid form to maximise mechanical properties. This results in a much longer fabrication time in comparison to the traditional non-foam infill design. A possible approach to mitigating this is to use a higher EM and lower infill percentage as the expansion of the foam material fills the gap between raster lines, resulting in solid foamed cores. As shown in Figure 3, the higher EM value cannot be chosen for foam PLA when the part has 100% infill due to extensive foam expansion, which causes huge over-extrusion and dimensional inaccuracy. However, lower infill percentages provide space in the middle of the part that can be filled by the foam expansion when the EM value is set at 0.9. Figure 12 (a) shows that the extruded cube with 80% infill and EM=0.9 experienced over-extrusion and dimensional inaccuracy above the acceptable tolerance (±0.5 mm) for the desktop MEX machines. However, both 20% and 50% infill are within the acceptable tolerance range. It is noteworthy to mention that the raster width is larger for 50% and 20% infill design in comparison to 80% and 100% infill design, as shown in Figure 12 (b). This can be justified by the available space in the lower infill, which allows the foam to expand to its full capacity, whilst in higher infill, due to limited space, the expansion overlaps with the previous raster line and causes over extrusion. The results suggest that there should be an optimum infill percentage for each deposition temperature or extrusion speed that controls the foaming expansion. However, to keep the discussion consistent, three infill percentages (20%, 50% and 80%) were chosen, the same as in the previous section.
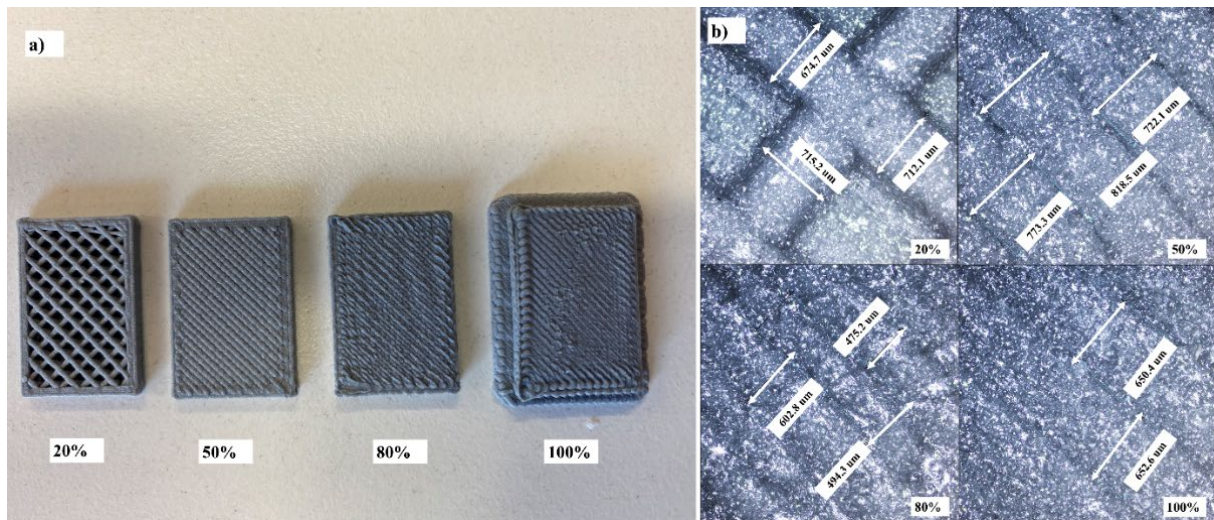

Figure 12: (a) Extruded foam PLA with EM of 0.9 and various infill (b) Microscopic image of the raster lines

Figure 13 (a) shows the density versus infill percentage plots for two different EM values. The density could not be calculated when EM and infill were set at 100% due to the cube's irregular shape, making it difficult to calculate the volume accurately. It is evident that the EM value directly affected density where extruded cubes with EM=0.9 have approximately x1.8 greater density than the cube with EM=0.5. The density of the extruded cube with processing parameters of 100% infill and EM=0.5 is close to the density of the cube with processing parameters of 50% infill and EM=0.9 (0.59 g/cc and

0.62 g/cc, respectively). However, there are noticeable differences in the strength and stiffness of these two process parameters (Figure 14).
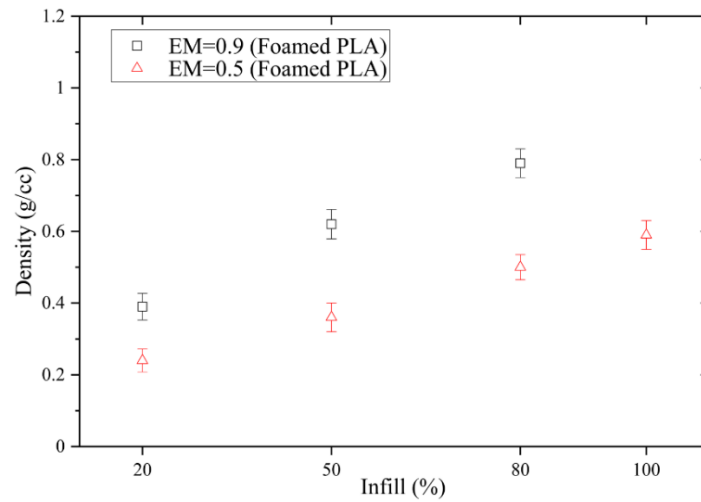

Figure 13: The effect of the EM and infill percentage on the density of extruded foam PLA

The average tensile strength and stiffness of the foamed specimens extruded with EM=0.9 and 50% infill were greater by 56% and 18%, respectively, in comparison to the solid foamed specimens extruded with EM=0.5. This can be justified as specimens with lower infill and higher EM values have fewer but thicker raster lines due to excessive foam expansion, as presented in Figure 12 (b). This is essentially similar to using the larger nozzle size, which allows more molten material to be deposited, filling the volume space of the product during the process (Triyono *et al.*, 2020). Conversely, the average compression yield strength and stiffness are lower by 15.4% and 14.1%, respectively, in foamed specimens with EM=0.9 than those extruded with EM=0.5.

Changing infill density from 50% to 20% reduced the average strength and stiffness moderately in foamed specimens extruded with EM= 0.9, contrary to the samples extruded with low EM, as shown in Figure 10 (b) and Figure 11 (b). The density of the extruded cube with 20% infill and EM=0.9 is similar to the density of the cube with 50% infill and EM=0.5 (0.39 g/cc and 0.36 g/cc, respectively). Despite this, the average tensile, compression and flexural yield strength in foamed specimens with 20% infill and EM=0.9 were higher by 65%, 15.5%, and 59%, respectively, than those printed with 50% infill and EM=0.5. For specimens printed with 20% infill and EM=0.9, the average stiffness follows a similar pattern, and it is higher by 13% in tensile, 11% in compression, and 50% in flexure compared to the specimens extruded with 50% infill and EM=0.5.
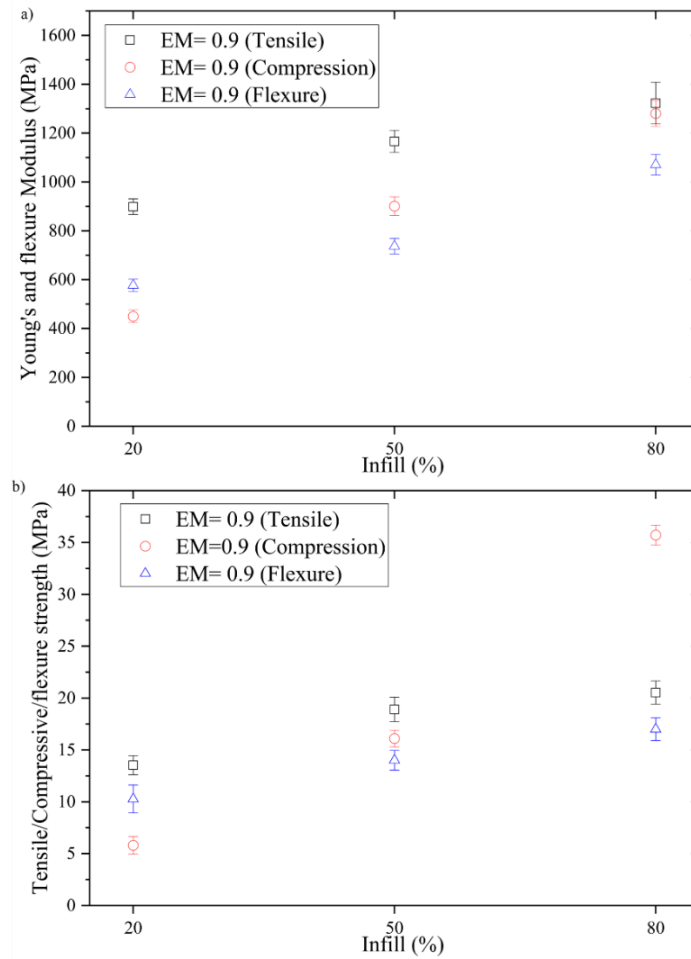
Figure 14: The (a) stiffness and (b) strength of printed foam samples when EM=0.9

The results suggest (Table 4) that using a lower infill percentage and a higher flow rate (EM=0.9) for foamed PLA provides higher strength and stiffness than those extruded with a higher infill percentage and lower flow rate (EM=0.5), while printed samples will have similar density. In addition, the former processing parameters require significantly less time than the latter process parameters due to fewer raster lines in the inner infill.

Table 4: The summary of the results for foam samples printed with two different EM in the YX direction

Infill %	EM	Tensile		Compression		Flexural	
		E (MPa)	σ_y (MPa)	E (MPa)	σ_y (MPa)	E (MPa)	σ_y (MPa)
100	0.9	--	--	--	--	--	--
	0.5	958 ± 15.9	8.20 ± 0.29	1028±23	19.0±0.65	878 ± 14	8.13 ± 0.3
80	0.9	1323±85	20.53±1.12	1280±52	35.71±0.95	1071±42	17±1.1
	0.5	879 ± 37	6.67±0.62	798±40	13.78±0.39	540±32	6.7±0.85
50	0.9	1166±45	18.91±1.18	901±38	16.1±0.8	737±32	14±4.62
	0.5	780 ± 30	4.62±0.92	400±27	4.9±0.1	288.6±21	4.2±0.64
20	0.9	899±32	13.53±0.92	450±26	5.8±0.85	577±25	10.27±1.3
	0.5	540±24	2.26±0.52	227±22	2.25±0.1	185.2±28	2.8±0.42

4. Conclusion:

In this work, various foamed and non-foamed PLA specimens were fabricated by changing nozzle temperature to create structures with different densities. The non-foamed PLA structures were produced at an extrusion temperature of 200 °C. Even though there is evidence of a small degree of foaming as blister-type structures can be observed on the extruded part at 200 °C, the samples at this temperature are considered to be non-foamed as there are not enough air bubbles to provide foamed characteristics.

The amount of foam expansion will be determined by the melt temperature and the amount of time the material remains foamable. To achieve optimal foam expansion, a balance must be established between an appropriate opportunity for foaming agent breakdown and pore nucleation and development. The maximum foaming expansion was achieved at 220 °C. The EM value had to be adjusted to compensate for foaming expansion and reach dimensional accuracy.

The surface roughness of the samples is affected by the amount of foaming expansion, the uniformity of the raster width, and the raster gap. When foaming occurred at temperatures over 200 °C, the profile and areal roughness values more than doubled as the blisters in foamed samples became near-spherical bubbles and widespread, resulting in a significantly roughened surface.

The deposition temperature of the polymer affected the mechanical properties of the extruded samples. In other words, temperature deposition affected foaming expansion in the PLA and varied the density of the part, which directly affected the mechanical properties. Regardless of the loading condition, the maximum stiffness and yield strength were obtained at 200 °C deposition temperature when there was no foam in the PLA specimens. In contrast, the stiffness and yield strength were reduced significantly when the maximum foaming occurred (220 °C deposition temperature) in the PLA specimens. The general trend of strength graphs for tensile and flexure tests shows that increasing the deposition temperature above 220 °C can improve properties slightly as the foaming expansion reduces in the raster lines. However, the compression properties almost remained constant at the higher temperature.

When the infill percentage was reduced, the compression and flexural yield strength decreased significantly in non-foamed PLA specimens compared to foamed PLA specimens. The slightly better performance of the lower infill foamed PLA samples under compressive load can be justified by the expanded structure of foam, which absorbed mechanical energy locally and reduced local buckling in the inner walls.

Extruding foamed PLA with a lower infill percentage and a higher flow rate delivers more strength and stiffness than with a higher infill percentage and a lower flow rate. Furthermore, due to fewer raster lines in the inner infill, the former processing parameters require substantially less time than the latter processing parameters for part manufacture.

Declaration of Competing Interest

The authors declare that they have no known competing financial interests or personal relationships that could have influenced the work reported in this paper.

References:

Abbott, A.C., Tandon, G.P., Bradford, R.L., Koerner, H. and Baur, J.W. (2018), "Process-structure-property effects on ABS bond strength in fused filament fabrication", *Additive Manufacturing*, Elsevier B.V., Vol. 19, pp. 29–38.

Bharath Kumar, B.R., Doddamani, M., Zeltmann, S.E., Gupta, N., Ramesh, M.R. and Ramakrishna, S. (2016), "Processing of cenosphere/HDPE syntactic foams using an industrial scale polymer injection molding machine", *Materials & Design*, Elsevier Ltd, Vol. 92, pp. 414–423.

Butscher, A., Bohner, M., Roth, C., Ernstberger, A., Heuberger, R., Doebelin, N., Rudolf Von Rohr, P., *et al.* (2012), "Printability of calcium phosphate powders for three-dimensional printing of tissue engineering scaffolds", *Acta Biomaterialia*, Acta Materialia Inc., Vol. 8 No. 1, pp. 373–385.

Chacón, J.M., Caminero, M.A., García-Plaza, E. and Núñez, P.J. (2017), "Additive manufacturing of PLA structures using fused deposition modelling: Effect of process parameters on mechanical properties and their optimal selection", *Materials & Design*, Elsevier Ltd, Vol. 124, pp. 143–157.

Choi, W.J., Hwang, K.S., Kwon, H.J., Lee, C., Kim, C.H., Kim, T.H., Heo, S.W., *et al.* (2020), "Rapid development of dual porous poly(lactic acid) foam using fused deposition modeling (FDM) 3D printing for medical scaffold application", *Materials Science and Engineering: C*, Elsevier, Vol. 110 No. September 2019, p. 110693.

Coste, G., Negrell, C. and Caillol, S. (2020), "From gas release to foam synthesis, the second breath of blowing agents", *European Polymer Journal*, Elsevier, Vol. 140 No. September, p. 110029.

D638-14, A. (2017), *Standard Test Method for Tensile Properties of Plastics*, ASTM International, available at:https://doi.org/10.1520/D0638-14.

D695-15, A. (2016), *Standard Test Method for Compressive Properties of Rigid Plastics*, ASTM International, available at:https://doi.org/10.1520/D0695-15.

D790-10, A. (2016), *Standard Test Methods for Flexural Properties of Unreinforced and Reinforced Plastics and Electrical Insulating Materials*, ASTM International, available at:https://doi.org/10.1520/D0790-10.

Damanpack, A.R., Sousa, A. and Bodaghi, M. (2021), "Porous PLAs with Controllable Density by FDM 3D Printing and Chemical Foaming Agent", *Micromachines*, Vol. 12 No. 8, p. 866.

Das, S., Heasman, P., Ben, T. and Qiu, S. (2017), "Porous Organic Materials: Strategic Design and Structure–Function Correlation", *Chemical Reviews*, Vol. 117 No. 3, pp. 1515–1563.

David Eaves. (2004), *Handbook of Polymer Foams*, Rapra Technology, Shawbury, U.K.

Gama, N., Ferreira, A. and Barros-Timmons, A. (2018), "Polyurethane Foams: Past, Present, and Future", *Materials*, Vol. 11 No. 10, p. 1841.

Górski, F., Kuczko, W., Wichniarek, R. and Hamrol, A. (2015), "Computation of Mechanical Properties of Parts Manufactured by Fused Deposition Modeling Using Finite Element Method", Springer, Cham, pp. 403–413.

Guddati, S., Kiran, A.S.K., Leavy, M. and Ramakrishna, S. (2019), "Recent advancements in additive manufacturing technologies for porous material applications", *The International Journal of Advanced Manufacturing Technology*, The International Journal of Advanced Manufacturing Technology, Vol. 105 No. 1–4, pp. 193–215.

Gupta, N. and Ricci, W. (2006), "Comparison of compressive properties of layered syntactic foams having gradient in microballoon volume fraction and wall thickness", *Materials Science and Engineering: A*, Vol. 427 No. 1–2, pp. 331–342.

H S, B., Bonthu, D., Prabhakar, P. and Doddamani, M. (2020), "Three-Dimensional Printed Lightweight Composite Foams", *ACS Omega*, Vol. 5 No. 35, pp. 22536–22550.

Hammel, E.C., Ighodaro, O.L.-R. and Okoli, O.I. (2014), "Processing and properties of advanced porous ceramics: An application based review", *Ceramics International*, Elsevier, Vol. 40 No. 10, pp. 15351–15370.

Hermann, S. (2020), "COLORFABB LW-PLA TESTING FOAMING PLA", available at: https://www.cnckitchen.com/blog/colorfabb-lw-pla-testing-foaming-pla (accessed 3 October 2021).

ISO/ASTM52921-13. (2019), *Standard Terminology for Additive Manufacturing—Coordinate Systems and Test Methodologies*, available at:https://doi.org/10.1520/ISOASTM52921-13R19.

Jayavardhan, M.L., Bharath Kumar, B.R., Doddamani, M., Singh, A.K., Zeltmann, S.E. and Gupta, N. (2017), "Development of glass microballoon/HDPE syntactic foams by compression molding", *Composites Part B: Engineering*, Elsevier Ltd, Vol. 130, pp. 119–131.

Jin, F.-L., Zhao, M., Park, M. and Park, S.-J. (2019), "Recent Trends of Foaming in Polymer Processing: A Review", *Polymers*, Vol. 11 No. 6, p. 953.

Kumar, S., Yan, J., Poon, J., Singh, V.P., Lu, X., Karlsson Ott, M., Engman, L., *et al.* (2016a), "Multifunctional Antioxidants: Regenerable Radical-Trapping and Hydroperoxide-Decomposing Ebselenols", *Angewandte Chemie*, Vol. 128 No. 11, pp. 3793–3797.

Kumar, S., Yan, J., Poon, J., Singh, V.P., Lu, X., Karlsson Ott, M., Engman, L., *et al.* (2016b), "Multifunctional Antioxidants: Regenerable Radical-Trapping and Hydroperoxide-Decomposing Ebselenols", *Angewandte Chemie*, Vol. 128 No. 11, pp. 3793–3797.

Naguib, H.E., Park, C.B. and Reichelt, N. (2004), "Fundamental foaming mechanisms governing the volume expansion of extruded polypropylene foams", *Journal of Applied Polymer Science*, Vol. 91 No. 4, pp. 2661–2668.

Reglero-Ruiz, A., Vincent, M., Agassant, J., Pillon, C., Carrot, C., Antonio, J., Ruiz, R., *et al.* (2015), "Polymer foaming with chemical blowing agents : Experiment and modeling To cite this version", *Polymer Engineering and Science*, pp. 2018–2029.

Singh, A.K., Saltonstall, B., Patil, B., Hoffmann, N., Doddamani, M. and Gupta, N. (2018), "Additive Manufacturing of Syntactic Foams: Part 2: Specimen Printing and Mechanical Property Characterization", *JOM*, Springer US, Vol. 70 No. 3, pp. 310–314.

Singh, S., Ramakrishna, S. and Singh, R. (2017), "Material issues in additive manufacturing: A review", *Journal of Manufacturing Processes*, The Society of Manufacturing Engineers, Vol. 25, pp. 185–200.

Song, P., Zhou, C., Fan, H., Zhang, B., Pei, X., Fan, Y., Jiang, Q., *et al.* (2018), "Novel 3D porous biocomposite scaffolds fabricated by fused deposition modeling and gas foaming combined technology", *Composites Part B: Engineering*, Elsevier, Vol. 152 No. April, pp. 151–159.

Stehr, J. (2016), "Chemical Blowing Agents in the Rubber Industry. Past – Present – and Future?", *International Polymer Science and Technology*, Vol. 43 No. 5, pp. 1–10.

Triyono, J., Sukanto, H., Saputra, R.M. and Smaradhana, D.F. (2020), "The effect of nozzle hole diameter of 3D printing on porosity and tensile strength parts using polylactic acid material", *Open Engineering*, Vol. 10 No. 1, pp. 762–768.

Wu, J., Chen, N., Bai, F. and Wang, Q. (2018), "Preparation of poly(vinyl alcohol)/poly(lactic acid)/hydroxyapatite bioactive nanocomposites for fused deposition modeling", *Polymer Composites*, Vol. 39 No. c, pp. E508–E518.

Yoo, C.J., Shin, B.S., Kang, B.S., Gwak, C.Y., Park, C., Ma, Y.W. and Hong, S.M. (2017), "A Study on a New 3D Porous Polymer Printing Based on EPP Beads Containing CO 2 Gas", *Procedia Engineering*, Vol. 184, pp. 10–15.